1   **Title: Apidima Cave (Greece): the earliest known *Homo sapiens* in Eurasia**

2   **Authors:** Katerina Harvati[1,2,10]*, Carolin Röding[1], Abel M. Bosman [1,2], Fotios A. Karakostis[1],

3   Rainer Grün[3], Chris Stringer[4], Panagiotis Karkanas[5], Nicholas C. Thompson[1,10], Vassilis

4   Koutoulidis[6], Lia A. Moulopoulos[6], Vassilis G. Gorgoulis[7,8,9]* & Mirsini Kouloukoussa[7,10]

5   **Affiliations:**

6   [1] Paleoanthropology, Senckenberg Centre for Human Evolution and Palaeoenvironment,

7   Eberhard Karls University of Tübingen, Rümelinstrasse 23, Tübingen 72070, Germany.

8   [2] DFG Centre of Advanced Studies 'Words, Bones, Genes, Tools', Eberhard Karls University of

9   Tübingen, Rümelinstrasse 23, Tübingen 72070, Germany.

10   [3] Australian Research Centre for Human Evolution, Griffith University, Nathan QLD 4111,

11   Australia

12   [4] Centre for Human Evolution Research, Department of Earth Sciences, The Natural History

13   Museum, London SW7 5BD, United Kingdom.

14   [5] Malcolm H. Wiener Laboratory for Archaeological Science, American School of Classical

15   Studies at Athens, Soudias 54, 10676, Athens, Greece.

16   [6] First Department of Radiology, National and Kapodistrian University of Athens, 76 Vas.

17   Sophias Ave, 11528, Athens, Greece.

18   [7] Department of Histology and Embryology, Medical School, National and Kapodistrian

19   University of Athens, 75 Mikras Asias Str, Goudi, 11527, Athens, Greece.

20   [8] Biomedical Research Foundation of the Academy of Athens, Athens, Greece.

21   [9] Faculty of Biology, Medicine and Health, University of Manchester, Manchester Academic

22   Health Science Centre, Manchester, United Kingdom.

23   [10] Museum of Anthropology, Medical School, National and Kapodistrian University of Athens,

24   75 Mikras Asias Str, Goudi, 11527, Athens, Greece.

25 **The two fossil human crania from Apidima, southern Greece, were discovered in 1978 but**

26 **have remained enigmatic due to their incomplete nature, taphonomic distortion and lack of**

27 **archaeological context and chronology. Here, we virtually reconstructed them, produced**

28 **their first exhaustive comparative descriptions and analyses, and dated them with the U-**

29 **series radiometric method. Apidima 2 dates to >170 ka and conforms to a Neanderthal-like**

30 **morphological pattern. In contrast, Apidima 1 dates to >210 ka and presents a mixture of**

31 **modern human and ancestral features. Results suggest the presence of two late Middle**

32 **Pleistocene human groups at this site, representing an early *Homo sapiens* population,**

33 **followed by a Neanderthal one. Our findings support multiple dispersals of early modern**

34 **humans out of Africa, and highlight the complex demographic processes that characterized**

35 **Pleistocene human evolution and modern human origins in South East Europe.**

36

37   South East Europe is considered a major dispersal corridor, and one of the principal European

38   Mediterranean glacial refugia [1,2,3]. As such, the region's human fossil record is proposed to be

39   more diverse than that of more isolated and less hospitable areas of Europe, reflecting the

40   complexities of repeated dispersals, late survivals and admixture of human groups [1,3]. This

41   hypothesis has been difficult to test, as paleoanthropological finds from the Balkans are

42   relatively scarce. The two fossil human crania from Apidima, Mani (Southern Greece) [4], are

43   among the most important finds from the region, yet remain little known. Here, we applied the

44   U-series dating method to elucidate their chronology and depositional history. We virtually

45   reconstructed both specimens, correcting for taphonomic damage, and consequently conducted

46   their first exhaustive comparative description and morphometric analyses.

47   **Chronology**

48   The Apidima specimens were discovered in 1978 in a block of breccia wedged high

49   between the cave walls of Apidima Cave A (Extended Data Fig. 1), during research by the

50   Museum of Anthropology, University of Athens School of Medicine. [2,4,5,6] Due to the lack of

51   associated context, their geological age has been difficult to assess. Attempts to date the site

52   radiometrically proved inconclusive [7]. However, geomorphology indicates a Middle-Late

53   Pleistocene age, with a bracket between 190-100 ka proposed as the most likely for the

54   deposition of the 'skull breccia' [6,8]. Previous work calculated a minimum age of ca. 160 ka by U-

55   series dating of an Apidima 2 bone fragment, suggesting a most likely time of deposition around

56   190 ka (transition between MIS 7 and MIS 6) [5].

57   We analyzed three samples from the 'skull breccia', selected from fragments produced

58   when cleaning the specimens from the matrix, with the U-series method. These included human

59   bone fragments (subsamples 3720A, B, Apidima 2; and subsamples 3754, 3755, Apidima 1) and

60   four unidentified bone subsamples (3757A-C, 3758, see Supplementary Information, section 1).

61   Our analyses show that both crania are older than the solidification of the matrix at around 150

62   ka. Despite their depositional proximity, Apidima 1 gained its uranium in a significantly

63   different environment than Apidima 2, during an accumulation event in MIS7 (around 210 ka),

64   while the U-uptake process of Apidima 2 took place in MIS 6 (around 170 ka) (Methods,

65   Supplementary Information, section 1). The crania and associated bones were therefore probably

66   trapped on the surface of the talus cone, Apidima 1 at around 210 ka and Apidima 2 at around

67   170 ka, and were brought to their final position before the cementation and solidification of the

68   sedimentary matrix at ca. 150 ka (Methods).

69   **Morphological Description and Comparative Analyses**

70   Apidima 2 (Fig. 1a-c, Extended Data Fig. 2) is the more complete and better known of

71   the crania, and has previously been considered an early Neanderthal or *Homo heidelbergensis*

72   [4,5,6,9]. It preserves an almost complete face and most of the vault (Supplementary Information,

73   section 2), but is taphonomically distorted. We produced four virtual manual reconstructions by

74   two observers following two different criteria from a CT scan of the original specimen (Extended

75   Data Figs. 3-4; Methods).

76   Apidima 1 (Fig. 1d-f) preserves the posterior cranium (Supplementary Information,

77   section 2). It shows no distortion, therefore its virtual reconstruction consisted of mirror imaging

78   the better-preserved side (Fig. 1e; Methods, Extended Data Fig. 5). It has been assumed to share

79   the same taxonomic attribution as Apidima 2 (e.g. [5]).

80   Apidima 2 shows Neanderthal-like features: a continuous, thick and rounded supraorbital

81   torus with no break between the glabellar, orbital and lateral regions; lack of break in plane

82   between the glabellar and lateral regions in superior view; anterior position of the nasal root;

83 inflated infraorbital region; bi-level morphology of the inferior nasal margin; and rounded '*en*

84 *bombe'* cranial profile in posterior view (Figs. 1a-c, Extended Data Figs. 2, 6, 7c-d). Most

85 standard measurements (Supplementary Table 2) align it with Neanderthals. We conducted

86 comparative geometric morphometric analyses of the face and neurocranium (Methods; Analyses

87 1-2, Fig. 2, Extended Data Table 1, Supplementary Tables 4-5), treating the Apidima 2

88 reconstructions and their mean configuration as individuals, projected into the PCA. In both

89 PCAs they plotted closest to Neanderthals or between Neanderthals and MPE. Linear

90 discriminant analyses (LDA) classified them as Neanderthal (except reconstruction 2, classified

91 as MPE only in Analysis 1; Extended Data Table 1). The overall shape of the Apidima 2

92 reconstruction mean was closest to Gibraltar 1 in Procrustes distance (PD) in the face, and to Spy

93 1 in the neurocranium, both Neanderthals.

94   In contrast, Apidima 1 does not show Neanderthal features; its linear measurements fall

95 mainly in the region of overlap between taxa (Supplementary Information, section 2,

96 Supplementary Table 3). It lacks a Neanderthal-like rounded '*en bombe'* profile in posterior view

97 (Figs. 1d, Extended Data Fig. 7a-b). The widest part of the cranium is relatively low on the

98 parietal; the parietal walls are nearly parallel and only slightly converge upwards, plesiomorphic

99 morphology common in Middle Pleistocene *Homo* [10,11]. It does not show the occipital plane

100 convexity and lambdoid flattening associated with Neanderthal occipital 'chignons'. Rather, its

101 midsagittal outline is rounded in lateral view, a feature considered derived for modern humans [12]

102 (Fig. 1e, Extended Data Fig. 7b). The superior nuchal lines are weak with no external occipital

103 protuberance. Unlike some Middle Pleistocene specimens, the occipital bone is not steeply

104 angled and lacks a thick occipital torus, (Figs. 1d-e, Extended Data Fig. 7a). A small, very faint,

105 depression is found above inion (length ca. 12 mm, height ca. 4.55 mm; Extended Data Fig. 7a).

106   Although suprainiac fossae are considered derived for Neanderthals [13], similar depressions occur

107   among modern humans and in some African early *H. sapiens* [14]. The Apidima 1 depression does

108   not present the typical Neanderthal combination of features. It is far smaller [15] and less marked

109   even than the 'incipient' suprainiac fossae of MPE specimens from Swanscombe and Sima de los

110   Huesos, being closest in size to the small supranuchal depression of the Eliye Springs MPA

111   cranium [16]. Apidima 1 therefore lacks derived Neanderthal morphology, instead showing a

112   combination of ancestral and derived modern human features.

113   We conducted a geometric morphometric analysis of the Apidima 1 neurocranium and its

114   midsagittal profile (Analyses 3 and 4; Fig. 3; Extended Data Table 1; Supplementary Tables 6-

115   7). In both analyses Apidima 1 clearly clustered with *H. sapiens* in the PCAs and was classified

116   as *H. sapiens* by the LDA (posterior probability 100 % and 93.4 %, Analyses 3 and 4,

117   respectively; Extended Data Table 1). Its overall shape was closest to Nazlet Khater 2 (Analysis

118   3) and Dolní Věstonice 3 (Analysis 4), both modern humans. We calculated a neurocranial shape

119   index based on the dataset from Analysis 3 following [17], using our Neanderthal and a modern

120   African sample (*n*=15; Methods) and projecting Apidima 1 and all other specimens onto this axis

121   (Fig. 3c). *H. sapiens*, both fossil and recent, are clearly separated from all archaic samples in this

122   index. Apidima 1 fell within the range of fossil *H. sapiens* and just outside that of modern

123   Africans, away from Neanderthals and MP samples. Interestingly, the MPA crania from Jebel

124   Irhoud, Morocco, considered early representatives of the *H. sapiens* lineage [18], plotted with

125   Neanderthals. The same analysis for the midsagittal profile dataset produced similar results

126   (Extended Data Fig. 8).

127   We compared the Apidima specimens for their common preserved anatomy. While

128   broadly similar in bi-auricular breadth, Apidima 2 is larger in its maximum cranial breadth,

129 reflecting its 'en bombe' outline in posterior view (Extended Data Figs. 6, 7c). Apidima 1 is

130 shorter antero-posteriorly and more rounded in lateral view (Extended Data Fig. 9). The analysis

131 of a restricted dataset of shared neurocranial landmarks and semilandmarks (Analysis 5; Fig. 4,

132 Extended Data Table 1, Supplementary Table 8) shows results similar to Analyses 1-4. The

133 Apidima 2 reconstructions fell with or close to Neanderthals along PC1-2 and were classified as

134 Neanderthal (Extended Data Table 1). Their mean was closest in overall shape to Saccopastore 1,

135 an early Neanderthal. Apidima 1 plotted closest to the *H. sapiens* convex hull, was classified as

136 *H. sapiens* (posterior probability 92%, Extended Data Table 1), and was closest to Nazlet Khater

137 2, a modern human, in PD.

138   **Implications for Human Evolution in South-east Europe**

139   Our assessment of the overall features, linear measurements and shape analyses of the

140 face and neurocranium of Apidima 2 support a Neanderthal or early Neanderthal attribution,

141 consistent with its chronological age of >170 ka under the 'accretion hypothesis' [19]. In contrast,

142 Apidima 1 lacks derived Neanderthal features despite postdating the establishment of the distinct

143 Neanderthal morphology [19]. Instead it shows a rounded posterior cranium, considered derived for

144 modern humans [12]. This morphology cannot be explained by ontogenetic age, sexual dimorphism

145 or interindividual variability. Although these factors might produce attenuated Neanderthal

146 characteristics, they should not result in a complete lack of Neanderthal occipital features [20,21],

147 nor in the presence of derived modern human traits. It might be hypothesized that Apidima 1

148 represents an early stage of the Neanderthal lineage, when facial morphology was established but

149 derived features of the posterior cranium were not [5,10]. However, Apidima 1 differs not only from

150 similarly dated early Neanderthals (e.g. Saccopastore, Biache-St-Vaast), but also from earlier

151 specimens from Sima de los Huesos, Swanscombe, and Reilingen, which exhibit Neanderthal-

152 like occipital features [19]. It also differs from MPE specimens like Petralona (Northern Greece) or

153 Ceprano, which show angulated occipitals and thickened tori, features absent in Apidima 1.

154 While the Steinheim MPE specimen appears somewhat rounded in lateral view, it is heavily

155 damaged, having suffered multidirectional distortions and erosion, making its morphology and

156 taxonomic attribution uncertain [14,22].

157   Apidima 1, therefore, does not fit in the 'accretional' scheme of Neanderthal evolution [19],

158 proposed as the main explanatory model of human evolution in Europe. Rather, its combination

159 of ancestral and derived modern human features and overall shape are consistent with an early

160 modern human taxonomic attribution. If this interpretation is correct, it documents the earliest

161 known presence of *Homo sapiens* in Eurasia, indicating that early modern humans dispersed out

162 of Africa starting much earlier, and reaching much further, than previously thought. It also

163 suggests that contact with the Neanderthal lineage may also have occurred during the Middle

164 Pleistocene, as postulated from ancient DNA evidence [23]. Together, the Apidima crania suggest a

165 complex pattern of population dispersal and possible replacement for southern Greece not unlike

166 that proposed for the Levant [24,25,26], a potential source area for the population represented by

167 Apidima 1. In such a scenario, early modern humans present in the region in the late Middle

168 Pleistocene were replaced by Neanderthals, whose subsequent presence in southern Greece is

169 well-documented [27,28,29]. The latter were themselves replaced by Upper Paleolithic modern

170 humans, whose earliest appearance in the region, as documented by Upper Paleolithic lithic

171 industries, dates to approximately 40 ka [30,31,32]. Our results highlight both the scarcity of our

172 knowledge of the human fossil record in South-East Europe and the importance of this region in

173 understanding Pleistocene human evolution and modern human origins.

As we completed this paper, we noted the publication of a new study of the Apidima 1 and 2 partial crania [33]. The authors of that study conclude that the two crania represent a transitional population between European *Homo erectus* and Neanderthals, a conclusion that is not supported by our more comprehensive analyses.

REFERENCES

1. Dennell, R.W., Martinón-Torres, M., Bermúdez de Castro, J.M. Hominin variability, climatic instability and population demography in Middle Pleistocene Europe. *Quat. Sci. Rev*. **30**, 1511-2524 (2011).

2. Tourloukis, V. & Harvati, K. The Palaeolithic record of Greece: a synthesis of the evidence and a research agenda for the future. *Quat. Int*. **466**, 48–65 (2018).

3. Roksandic, M., Radović, P. & Lindal J. Revising the hypodigm of *Homo heidelbergensis*: A view from the Eastern Mediterranean. *Quat. Int.* **466**, 66–81 (2018).

4. Pitsios, T. K. Paleoanthropological research at the cave site of Apidima and the surrounding region (south Peloponnese, Greece). *Anthropol Anzeiger* **57**, 1–11 (1999).

5. Bartsiokas, A., Arsuaga, J. L., Aubert, M. & Grün, R. U-series dating and classification of the Apidima 2 hominin from the Mani peninsula, Southern Greece. *J. Hum. Evol.* **109**, 22–29 (2017).

6. Harvati, K., Stringer, C. & Karkanas, P. Multivariate analysis and classification of the Apidima 2 cranium from Mani, Southern Greece. *J. Hum. Evol.* **60**, 246–250 (2011).

7. Liritzis, Y. & Maniatis, Y. ESR experiments on quaternary calcites and bones for dating purposes. *J. Radioanalytical Nuclear Chem.* **12**, 30−21 (1989).

197   8. Rondoyanni, T., Mettos, A. & Georgiou, C. Geological-morphological observations in

198   the greater Oitilo-Diros area, Mani. *Acta Anthropol.* **1**, 93–102 (1995).

199   9. Coutselinis, A., Dritsas, C. & Pitsios, T. K. Forensic investigation of the Pleistocene skull

200   LAO 1/S2 (Apidima II), Apidima, Laconia, Greece. *Anthropologie* **95**, 401–408 (1991).

201   10. Arsuaga, J. L. *et al.* Neandertal roots: Cranial and chronological evidence from Sima de

202   los Huesos. *Science* **344**, 1358–1363 (2014).

203   11. Stringer, C. The origin and evolution of *Homo sapiens*. *Phil. Trans. R. Soc. B* **371**,

204   20150237 (2016).

205   12. Galway-Witham J. & Stringer C. How did Homo sapiens evolve? *Science* **360**, 1296-

206   1298 (2018).

207   13. Harvati, K. in *Handbook of Paleoanthropology* (eds Henke, W. & Tattersall, I.) 2243–

208   2279 (Springer, 2015).

209   14. Balzeau, A. & Rougier, H. Is the suprainiac fossa a Neandertal autapomorphy? A

210   complementary external and internal investigation. *J. Hum. Evol.* **52**, 1-22 (2010)

211   15. Verna, C., Hublin, J. – J., Debenath, A., Jelinek, A. & Vandermeersch, B. Two new

212   hominin cranial fragments from the Mousterian levels at La Quina (Charente, France). *J.*

213   *Hum. Evol.* **58**, 273–278 (2010).

214   16. Bräuer, G. & Leakey, R. L. The ES-11693 cranium from Eliye Springs, West Turkana,

215   Kenya. *J. Hum. Evol.* **15**, 289–312 (1986).

216   17. Gunz, P. *et al*. Neandertal introgression sheds light on modern human endocranial

217   globularity. *Current Biology* **29**, 120-127 (2019).

218   18. Hublin, J.-J. *et al*. New fossils from Jebel Irhoud (Morocco) and the Pan-African origin

219   of *Homo sapiens. Nature* **546**, 289-292 (2017).

220 19. Hublin, J. – J. The origin of Neandertals. *Proceedings of the National Academy of*

221   *Sciences (USA)* **106**, 16022–16027 (2009).

222 20. Caspari, R. The Krapina occipital bones. *Period. Biol.* **108**, 299–307 (2006).

223 21. Arsuaga, J. L., Martínez, I., Gracia, A. & Lorenzo, C. The Sima de los Huesos crania

224   (Sierra de Atapuerca, Spain). A comparative study. *J. Hum. Evol.* **33**, 219–281 (1997).

225 22. Prossinger, H., Seidler, H., Wicke, L., Weaver, D., Recheis, W., Stringer, C. & Müller,

226   G.B. Electronic removal of encrustations inside the Steinheim cranium reveals paranasal

227   sinus features and deformations, and provides a revised endocranial volume estimate.

228   *Anat. Rec*. **273b**, 132-142 (2003).

229 23. Posth, C. *et al*. Deeply divergent archaic mitochondrial genome provides lower time

230   boundary for African gene flow into Neanderthals. *Nature Communications* **8**, 16046

231   (2017).

232 24. Mercier, N. *et al*. Thermoluminescence date for the Mousterian burial site of Es-Skhul,

233   Mt. Carmel. *J. Archaeol. Sci.* **20**, 169–174 (1993).

234 25. Hershkovitz, I. *et al*. The earliest modern humans outside Africa. *Science* **359**, 456–459

235   (2018).

236 26. Stringer, C., Galway-Whitham, J. When did modern humans leave Africa?. *Science* **359**,

237   389–390 (2018).

238 27. Harvati, K., Panagopoulou, E., Karkanas, P. First Neanderthal remains from Greece: The

239   evidence from Lakonis. *J. Hum. Evol.* **45**, 465-473 (2003).

240 28. Harvati, K., *et al*. New Neanderthal remains from Mani peninsula, S. Greece: The

241   Kalamakia Middle Palaeolithic cave site. *J. Hum. Evol.* **64**, 486-499 (2013).

242 29. Tourloukis, V., *et al*. New Middle Paleolithic sites from the Mani peninsula, Southern

243   Greece. *Journal of Field Archaeology* **41**, 68-83 (2016).

244   30. Elefanti, P., Panagopoulou, E., Karkanas, P. The transition from the Middle to the Upper

245   Paleolithic in the Southern Balkans: the evidence from Lakonis 1 Cave, Greece. *Eurasian*

246   *Prehistory* **5**, 85-95 (2008).

247   31. Douka, K., Perlès, C., Valladas, H., Vanhaeren, M., Hedges, R.E.M. Francthi Cave

248   revisited: the age of the Aurignacian in south-eastern Europe. *Antiquity* **85**, 1131-1150

249   (2011).

250   32. Lowe, J., *et al*. Volcanic ash layers illuminate the resilience of Neanderthals and early

251   modern humans to natural hazards. *Proceedings of the National Academy of Sciences*

252   *(USA)* **109**, 13532-13537 (2012).

253   33. De Lumley, M.A. *Les restes humains anténéanderthaliensis Apidima 1 et Apidima 2*

254   (CNRS, 2019)

255

256   **Supplementary Information** is available in the online version of the paper.

257

279 **Figure 1. Apidima 2 and 1.** Apidima 2, panels: **a,** Frontal view. **b,** Right lateral view. **c,** Left

280 lateral view. Apidima 1, panels: **d,** Posterior view. **e,** Lateral view. **f,** Superior view. Scale = 5

281 cm.

282

283 **Figure 2. PCA of Apidima 2 (Analyses 1-2): a,** Analysis 1, PCA of Procrustes-superimposed

284 facial landmarks, PC1 vs PC2. *H. sapiens*, blue triangles ($n = 19$), Neanderthals, red stars ($n = 6$),

285 MPE, yellow squares ($n = 3$), MPA, purple squares ($n = 3$). PC1 shape changes shown below the

286 plot reflect the modern human flat, small-browed face (positive) vs the forward projecting, large

287 nose and large browridge of Neanderthals (negative). **b,** Analysis 2, PCA of Procrustes-

288 superimposed neurocranial landmarks and semilandmarks, PC1 vs PC2. *H. sapiens* ($n = 25$),

289 Neanderthals ($n = 8$), MPE ($n = 3$), MPA ($n = 5$), Apidima reconstructions, black polygons,

290 Apidima reconstruction mean configuration, black star. PC1 shape changes: modern human-like

291 rounded braincase (positive) vs low braincase with large arching browridges (negative).

292 Specimen abbreviations in Supplementary Table 9.

293

294 **Figure 3. Apidima 1 (Analyses 3-4). a,** Analysis 3, PCA of Procrustes-superimposed

295 neurocranial landmarks and semilandmarks, PC1 vs PC2. *H. sapiens* ($n = 23$), Neanderthals ($n = $

296 6), MPE ($n = 4$) and MPA ($n = 5$). PC1 shape changes shown below the plot: round, high,

297 relatively narrow (negative) vs low, elongated, wide cranium (positive). **b,** Analysis 4. PCA of

298 Procrustes-superimposed midsagittal neurocranial landmarks and semilandmarks, PC1 vs PC2.

299 *H. sapiens* ($n = 27$), Neanderthals ($n = 10$), MPE ($n = 5$) and MPA ($n = 6$). PC1 shape changes

300 reflect the relative contributions of the parietal / occipital bones to the midsagittal profile. PC2

301 shape changes shown next to the plot reflect round, high (positive) vs flat, elongated profiles

302 (negative). **c,** Neurocranial shape index (Analysis 3). Violins extend from the minimum to the

303 maximum value; boxes show the 25-75 % quartiles and lines the median. Samples as in Fig. 3a,

304 symbols as in Fig. 2; recent Africans, green dots (*n* = 15).

305

306 **Figure 4. Apidima 1 and 2 combined PCA (Analysis 5).** PCA of Procrustes-superimposed

307 neurocranial landmarks and semilandmarks shared between Apidima 1 and 2. PC1 vs PC2. *H.*

308 *sapiens* (*n* = 23), Neanderthals (*n* = 6), MPE (*n* = 4) and MPA (*n* = 5). Shape changes along PC1

309 (below the plot) reflect relatively narrow and high crania with curved parietal midsagittal

310 outlines in modern humans (positive) vs relatively wide, low crania with flat parietal midsagittal

311 profiles (negative). Positive PC2 scores reflect relatively curved parietals combined more

312 posterior parietal notch relative to auriculare. Symbols as in Fig. 2.

313

314 **METHODS**

315 **Depositional context.** The crania were discovered in 1978 encased in a small block of breccia

316 (65 cm x 45 cm x 35 cm) [34] wedged between the walls and near the ceiling of Apidima Cave A

317 (Extended Data Fig. 1). Bartsiokas et al.[5] calculated a minimum age of ca. 160 ka for a bone

318 fragment from Apidima 2 by U-series dating, thus constraining the upper limit of this range, and

319 proposed a most likely time of deposition around 190 ka (transition between MIS 7 and MIS 6) [5].

320 The breccia block is interpreted as a remnant of an eroded steep talus cone that originally fanned

321 out of the cliffs in front and above the cave (Extended Data Fig. 1c) [6]. The talus had to be graded

322 to a previously existing dryland surface, implying that sea level was much lower for most of the

323 time of its formation, most likely during a glacial period.

324   The U-series results (Supplementary Information, section 1) show that both human

325   samples are older than the solidification of the matrix at around 150 ka. This completely concurs

326   with common sense. Apidima 1 accumulated its uranium in a significantly different environment

327   than Apidima 2, during an accumulation event in MIS7 (around 210 ka) while the U-uptake

328   process of Apidima 2 took place in MIS 6 (around 170 ka). The crania and associated bones were

329   probably trapped on the surface of the talus cone, first Apidima 1 at around 210 ka and later

330   Apidima 2 at around 170 ka. The two crania were then brought into their final position at a later

331   time, before the cementation and solidification of the sedimentary matrix at ca. 150 ka. Water

332   preferentially infiltrating along cave walls often produces sediment dissolution and down-

333   washing, and formation of open spaces between the cave walls and the sedimentary fill. These

334   sedimentary traps are later filled with collapsed material from the overlying sedimentary

335   sequence. The location of the finds, between the walls of Apidima Cave A, wedged near the

336   ceiling, suggest a similar scenario where bone material from Apidima 2 could be dislocated in a

337   sedimentary trap from the overlying sequence and mix with Apidima 1 remains, that also entered

338   the trap at a later stage. The bones seem to have been thoroughly mixed, perhaps by a mudflow

339   creeping down the sedimentary trap before consolidating at ca. 150 ka.

340   **CT scanning and virtual manual reconstruction.**

341   The Apidima 1 and 2 crania were scanned at the First Department of Radiology of the National

342   and Kapodistrian University of Athens using a multidetector CT scanner (Philips, Best, The

343   Netherlands). The scanning parameters were as follows: tube voltage 120 kV, tube current-time

344   product 599 mAs, 16 × 0.75 collimation, 0.8 mm slice thickness, slice increment 0.4 mm, field of

345   view 249 mm, matrix 768 × 768, pitch 0.44, rotation time 0.75 s, convolution kernel detailed

346 (D), and ultra high focal spot resolution. The CT scans of both individuals show isotropic pixel

347 sizes of 0.31 and 0.32 mm respectively.

348   Apidima 1 and 2 were virtually reconstructed by A.M.B. and C.R. In all cases, the

349 reconstruction was manual and based on the preserved anatomical features. All reconstruction

350 steps were carried out in the software environment of Avizo (Visualization Sciences Group).

351 Prior to the multiple reconstructions of Apidima 2, each fragment was segmented separately to

352 allow independent movement during the virtual reconstructions (Extended Data Figs. 3-4).

353 Several thin and tiny fragments could not be segmented in a reproducible way due to minimal

354 differences in the grey values of bone and sediment matrix and were thus excluded from the

355 reconstructions. In total, 66 fragments were segmented. It was possible to segment fragments of

356 the posterior neurocranium with semi-automated processes, as there were sufficient density

357 differences between bone and matrix in this area. Facial fragments were mostly segmented

358 manually slice by slice, due to small differences in density between bone and matrix, combined

359 with a low thickness of the fragments.

360   Four independent reconstructions of Apidima 2 were carried out by A.M.B. and C.R.,

361 each using two different protocols (for comparison, see [35]). Independent of the protocol used,

362 matrix-filled cracks were not closed completely in the reconstructions, in order to account for

363 possible alterations of the edges of the fragments. No reference cranium was used during the

364 reconstructions of Apidima 2, in order to exclude the risk of driving the results in the direction of

365 the chosen reference specimen.

366   A shared feature of vertebrate crania is approximate bilateral symmetry. The first

367 protocol was based on this principle and had the goal to restore this symmetry. The anterior right

368 part of the neurocranium was chosen as a starting point, as it presented a low amount of

369   taphonomic deformation. Fragments of the right neurocranium were reconstructed according to a

370   biologically meaningful position relative to each other. All reconstructed fragments of the right

371   side were duplicated and mirrored along the midsagittal plane onto the left side. This mirrored

372   duplicate was used as reference for the reconstruction of the fragments from the distorted left

373   side of the neurocranium. The reconstructed left side of the brain case was subsequently mirrored

374   to the right side to reconstruct the missing right temporal bone. Following the same procedure,

375   the area close to the midsagittal plane on the right and a part of the supraorbital region on the left

376   were reconstructed (shown as grey areas in Extended Data Figs. 3-4). For restoring facial

377   symmetry, the midsagittal plane of the neurocranium was used as a reference. The right facial

378   side was reconstructed and mirrored to reconstruct the fragmented left side. The left nasal bone,

379   right maxilla-zygomatic fragment, and the left side of the lower face were duplicated and

380   mirrored to reconstruct missing areas (shown as grey areas in Extended Data Figs. 3-4).

381   The second protocol exploited the assumption that the ectocranial surface should follow a

382   smooth curvature, especially in the neurocranium. In this protocol, each fragment is spatially

383   constrained by its neighboring fragments. The anterior right part of the neurocranium was chosen

384   as a starting point, as several fragments were located in positions relative to each other that

385   almost preserved smooth curvature. After reconstructing the vault, the facial fragments were

386   repositioned relative to each other to match the smoothness criterion. However, mirroring of the

387   right side was necessary to check and correct the fragmented left side. When the position of

388   fragments had to be corrected in order to deal with taphonomic distortion, smoothness was

389   prioritized over bilateral symmetry. Finally, missing areas, such as the right temporal bone, the

390   right nasal bone, and the left maxilla were reconstructed by duplicating and mirroring their

391   preserved counterpart (shown as grey areas in Extended Data Figs. 3-4).

392   As shown previously [36,37], multiple reconstructions of the same specimen will typically

393   show some shape differences and no single reconstruction can be considered as 'perfect'. As the

394   different reconstructions might be considered equally plausible [36], we treated them as separate

395   individuals in all geometric morphometric analyses. Furthermore, we calculated the mean

396   configuration of all four reconstructions and treated this as an additional individual in our

397   analysis. The final Apidima 2 reconstructions retain some distortion with respect to the

398   relationship between the face and the neurocranium. Therefore, these two anatomical regions

399   were analyzed separately (see below, Comparative samples).

400   The reconstruction of Apidima 1 was carried out by first computing a plane though the

401   preserved part of the midsagittal suture. The slices of the CT scan were resampled according to

402   this computed plane. Subsequently, preserved parts of the right parietal bone and right side of the

403   occipital bone were cropped out along the computed plane in the original scan volume. This

404   allowed mirroring a duplication of the cropped scan volume along the midsagittal plane. As a

405   result, the reconstruction of Apidima S1 is completely symmetrical (Extended Data Fig. 5).

406   Figures of the reconstructions were produced in Adobe Photoshop.

407

408   **Comparative samples.** The samples used for our analyses included Neanderthals (MIS8-3),

409   earlier Middle Pleistocene specimens from Africa (MPA) and Eurasia (MPE), *H. sapiens*

410   (including early anatomically modern human specimens and Upper Paleolithic modern humans),

411   and recent Africans (n = 15) from the University of Witwatersrand Dart Collection. Severely

412   taphonomically distorted and pathological specimens were excluded. The comparative summary

413   statistics of the linear measurements reported in Supplementary Tables 2 and 5 were based on

414   data collected by C.S., supplemented by published values and by values collected on the

415   Tübingen paleoanthropology scan collection by K.H. and C.R. in Avizo (Visualization Sciences

416   Group). The geometric morphometric comparative data were collected by K.H. Linear and 3-D

417   measurements on the Apidima reconstructions were collected by K.H. and C.R. in Avizo

418   (Visualization Sciences Group).

419   Analysis 1: Apidima 2 face. This analysis comprised 25 facial landmarks: postorbital

420   sulcus, glabella, nasion, infraspinale, prosthion, mid torus superior right and left, mid torus

421   inferior right and left, dacryon right and left, zygoorbitale right and left, frontomalare right and

422   left, infraorbital foramen right and left, zygomaxillare right and left, alare right and left, jugale

423   right and left, frontomalare posterior right and left (for landmark definitions see [38]). Comparative

424   samples included 31 individuals: Middle Pleistocene Eurasians (MPE): Arago 21 (as

425   reconstructed by [36]), Petralona, Sima de los Huesos 5; Middle Pleistocene Africans (MPA):

426   Bodo, Broken Hill, Irhoud 1, Neanderthals: La Chapelle-aux-Saints, Gibraltar 1, Guattari, La

427   Ferrassie 1, Shanidar 1 and 5; *H. sapiens*: Abri Pataud, Chancelade, Cro-Magnon 1, 2, Dolní

428   Věstonice 3, 13, 14, 15 and 16, Grimaldi, Hofmeyr, Mladeč 1, Muierii 1, Oase 2, Předmostí 3

429   and 4, Qafzeh 6 and 9, Wadi Kubbaniya.

430   Analysis 2: Apidima 2 neurocranium. This analysis included landmarks and curve

431   semilandmarks outlining the supraorbital torus and midsagittal profile: glabella, bregma, lambda,

432   frontomalare posterior (FMLP) right and left; 26 semilandmarks from glabella to bregma; 18

433   semilandmarks from FMLP right to FMLP left. Comparative samples included 41 specimens:

434   MPE: Dali, Petralona, Sima de los Huesos 5; MPA: Broken Hill, Elandsfontein, Irhoud 1 and 2,

435   Omo 2; Neanderthals: Amud 1, La Chapelle-aux-Saints, Feldhofer, La Ferrassie 1, Guattari, La

436   Quina 5, Spy 1 and 2; *H. sapiens*: Abri Pataud, Brno, Chancelade, Cioclovina, Cro-Magnon 1, 2

437   and 3, Dolní Věstonice 3, 13, 15 and 16, Mladeč 1, 2 and 5, Muierii 1, Oase 2, Ohalo 2, Pavlov,

Předmostí 3 and 4, Qafzeh 6 and 9, Skhul 5, Zhoukoudian Upper Cave 101 and 103. For Mladeč

2, the FMLP points were reconstructed using the entire sample as reference (see Data

processing).

Analysis 3: Apidima 1 neurocranium. This analysis comprised 30 neurocranial landmarks

and semilandmarks, including bregma, lambda, inion, as well as parietal notch, auriculare and

porion bilaterally, and 21 semilandmarks from bregma to inion. Although the Apidima 1 parietal

is nearly complete in the midsagittal plane, bregma is not preserved and was reconstructed on the

basis of the entire fossil sample (see Data processing) in this and the next two datasets. The

comparative sample comprised 38 fossil individuals: MPE: Dali, Petralona, Reilingen, Sima de

los Huesos 5; MPA: Broken Hill, Eliye Springs, Irhoud 1 and 2, Omo 2; Neanderthals: Amud 1,

La Chapelle-aux-Saints, La Ferrassie 1, Guattari, La Quina 5, Saccopastore 1; *H. sapiens*: Abri

Pataud, Brno, Chancelade, Cioclovina, Cro-Magnon 1 and 2, Dolní Věstonice 3, 13, 15 and 16,

Mladeč 1and 5, Muierii 1, Nazlet Khater 2, Oase 2, Ohalo 2, Pavlov, Předmostí 3 and 4, Qafzeh

6 and 9, Skhul 5, Zhoukoudian Upper Cave 101.

Analysis 4: Apidima 1 midsagittal profile. This analysis comprised 24 landmarks and

semilandmarks outlining the midsagittal profile from bregma to inion in order to analyze the

parietal and occipital plane convexity of Apidima 1. The landmarks bregma, lambda, inion, and

21 semilandmarks from bregma to inion were included. The comparative sample numbered 48

individuals: MPE: Dali, Petralona, Reilingen, Sima de los Huesos 5, Swanscombe, MPA: Broken

Hill, Elandsfontein, Eliye Springs, Irhoud 1, 2, Omo 2; Neanderthals: Amud 1, Biache-st-Vaast,

La Chapelle-aux-Saints, Feldhofer, La Ferrassie 1, Guattari, La Quina 5, Saccopastore 1, Spy 1

and 2; *H. sapiens*: Aduma, Abri Pataud, Brno, Chancelade, Cioclovina, Cro-Magnon 1, 2 and 3,

460   Dolní Věstonice 3, 13, 15, 16, Mladeč 1 and 5, Muierii 1, Nazlet Khater 2, Oase 2, Ohalo 2, Omo

461   1, Pavlov, Předmostí 3 and 4, Qafzeh 6 and 9, Skhul 5, Zhoukoudian Upper Cave 101 and 103.

462   Analysis 5: Apidima 1 and 2 shared landmarks and semilandmarks. This analysis

463   included bregma, lambda, as well as parietal notch and auriculare (bilaterally), and 10

464   semilandmarks from bregma to lambda. The sample was the same as in Analysis 3, but

465   additionally comprised the Apidima 2 reconstructions.

466   **Data processing.** The fixed landmarks (Type I, II and III) and curve semilandmarks (Type IV)

467   were collected from the reconstructions in Avizo 9.2.0 Lite (Visualization Sciences Group). The

468   comparative data were collected by K.H. [37,38] and processed with the DVLR (dorsal-ventral-left-

469   right fitting) program (http://www.nycep.org/nmg/programs.html). The curve semilandmarks

470   were calculated by resampling each curve as a predetermined number of equally spaced points,

471   using Resample.exe (http://www.nycep.org/nmg/programs.html). As bregma was not present in

472   Apidima 1, but most of the bregma-lambda curve was preserved, this point was estimated using

473   Generalized Procrustes Analysis (GPA) mean substitution in Morpheus [39]. This protocol first

474   performs GPA to align the specimens. Then, grand-mean coordinate values are computed for the

475   missing landmark using the non-missing points. The inverse scale, rotation, and translation are

476   subsequently applied to restore the original data. The same procedure was used to reconstruct

477   frontomalare temporale for Mladeč 2 in Analysis 2 (Apidima 2 neurocranium). For the important,

478   taphonomically deformed specimen Arago 21 the virtual reconstruction produced by Gunz et al.

479   [36] was used in the comparative facial analysis of Apidima 2 (Analysis 2). Minimal reconstruction

480   based on the surrounding anatomy was allowed during data collection, and landmarks missing on

481   one side were reconstructed through reflected relabeling (Mardia et al.) [40], or by using a function

482   in R [41] based on Claude [42]. This function estimates a mirroring plane, based on the unilateral

483   landmarks. The missing landmarks are then reflected according to this plane. Subsequent to the

484   reconstruction of missing landmarks, the semilandmarks were slid along their respective closed

485   curves using the Morpho package [43] in R. Sliding was performed using the minimized bending

486   energy algorithm [44]. After sliding, the data were exported in Morphologika format for further

487   analysis [45].

488   **Data analysis.** The datasets compiled were imported in Morphologika [45] and superimposed

489   using GPA, which translates the specimen configurations to common origin, scales them for size

490   and rotates them to best fit. Procrustes distances among specimens are a measure of overall shape

491   difference. The superimposed coordinates of the comparative samples, excluding the Apidima

492   specimens, were used as variables in a PCA, performed in the Past 3.04 software [46]. The resulting

493   eigenvectors (PC loadings) were used to compute the PC scores for the Apidima specimens so as

494   to plot them into the PCA graphs after the latter had been calculated on the comparative samples

495   alone. PCA plots were processed using Adobe Illustrator and extracted as Adobe .pdf files.

496   Further, LDA and classification analyses were performed in Past 3.04 using the PCs as variables,

497   in each case treating the Apidima 1 and 2 reconstructions as unknown. The number of PCs

498   included in the LDA for each of the five analyses included the first 7, 8, 8, 4 and 4 PCs,

499   accounting for 70.72 %, 91 %, 88.6 %, 85.4 % and 78.2 % of the total variance, respectively.

500   Posterior probabilities were calculated with the SPSS software package (IBM Inc., Armonk, NY,

501   version 24 for Windows). We investigated whether the datasets used met the LDA assumptions

502   [47]. We verified that all variables (PC scores) showed an approximately normal distribution on the

503   basis of both histograms and normal probability plots [47]. We removed potential outliers from the

504   analysis by excluding pathological or taphonomically distorted specimens. Based on z-scores [47]

505   outliers were absent in all variables, except for one case in PC3 of Analysis 2: the MPA

506   individual Omo 2, whose z-score was 0.08 points over the maximum acceptable limit of 3.29 [47].

507   Given the limited number of well-preserved MPA crania in the fossil record, we decided to

508   maintain this specimen in the analysis so as to maximize this group's representation. Finally, the

509   covariance matrices were similar among groups in all analysis, and Box's M tests showed that

510   they were homogeneous for the samples used in Analyses 4 and 5 [47]. However, this assumption

511   could not be tested using Box's M for most analyses due to the small sample sizes of certain

512   fossil groups, a common problem in paleontology (e.g. [48]). Because of these limitations, the

513   results of the LDAs must be approached with caution, and not be interpreted in isolation, but in

514   the context of all analyses presented here.

515   **Visualization.** Shape changes along principal components axes were visualized in Morphologika

516   [45]. To further aid in visualization of shape differences between Apidima 1 and 2, as well as

517   Apidima 1 and other specimens (Extended Data Figs 9, Supplementary Fig. 3), we conducted

518   manual superimpositions of 3D models in the software environment of Avizo 9.2.0 Lite

519   (Visualization Sciences Group). In order to keep the superimpositions comparable, the different

520   comparative specimens stayed in their original configuration and manipulations were carried out

521   on the common component, in this case Apidima 1. In the first step of superimposition, Apidima

522   1 was scaled to the biauricular breadth of the comparative specimen. The transmeatal axes of

523   both specimens were matched by translating and rotating Apidima 1. In the last step, Apidima 1

524   was rotated around the transmeatal axis to match the orientations of the external auditory meatus

525   and the supramastoid crest of the comparative specimen.

526   **Shape index**: The globular shape of the modern human neurocranium is considered derived for

527   modern humans and differentiates them from Neanderthals and other archaic *Homo*. Gunz et al.

528   (2019) [17] recently showed that a less globular cranial shape in modern Europeans is related to the

529   presence of specific Neanderthal alleles in their genome. We calculated the shape index for the

530   posterior neurocranium of Apidima 1, to approximate the globularization index of [17]. We

531   calculated an axis between the mean shapes of our Neanderthal sample and a Neanderthal-

532   unadmixed, modern African sample (Zulu, Dart Collection, University of the Witwatersrand, $n =$

533   15), and projected all other specimens (Apidima 1, MPE, MPA and fossil *H. sapiens*) onto this

534   axis, to further evaluate the degree of globularity of the Apidima 1 neurocranium.

535   **Data availability.** The data that support the findings of this study will be made available from

536   the corresponding authors upon reasonable request.

537

538   34. Kormasopoulou-Kagalou, L., Protonotariou-Deilaki, E. & Pitsios, T. K. Paleolithic skull

539   burials at the cave of Apidima. *Acta Anthropol.* **1**, 119–124 (1995).

540   35. Zollikofer, C.P. *et al.* Virtual cranial reconstruction of *Sahelanthropus tchadensis. Nature*

541   **434**(7034), 755-759 (2005).

542   36. Gunz, P. *et al.* Principles for the virtual reconstruction of hominin crania. *J. Hum. Evol.*

543   **57**, 48-62 (2009).

544   37. Harvati, K., Hublin, J. – J. & Gunz, P. Evolution of Middle-Late Pleistocene human

545   cranio-facial form: A 3-D approach. *J. Hum. Evol.* **59**, 445−464 (2010).

546   38. Harvati, K., Gunz, P. & Grigorescu, D. Cioclovina (Romania): affinities of an early

547   modern European. *J. Hum. Evol.* **53**, 732−746 (2007).

548   39. Slice, D. *Morpheus et al., Java Edition* (The Florida State University, 2013).

549   40. Mardia, K. V., Bookstein, F. L. & Moreton, I. J. Statistical Assessment of Bilateral

550   Symmetry of Shapes. *Biometrika* **87**, 285−300 (2000).

551   41. R Development Core Team. *R: A language and environment for statistical computing* (R

552   Foundation for Statistical Computing, 2008).

553   42. Claude, J. *Morphometrics with R* (Springer Science & Business Media, 2008).

554   43. Schlager, S. in *Statistical Shape and Deformation Analysis* (eds Zheng, G., Li, S. &

555   Szekely, G.) 217−256 (Academic Press, 2017).

556   44. Bookstein, F. L. Landmark methods for forms without landmarks: morphometrics of

557   group differences in outline shape. *Med. Image Anal.* **1**, 225−243 (1997).

558   45. O'Higgins, P & Jones, N. *Morphologika 2.2. Tools for shape analysis* (Hull York

559   Medical School, 2006).

560   46. Hammer, Ø., Harper, D. A. T. & Ryan, P. D. PAST: Paleontological statistics software

561   package for education and data analysis. *Palaeontol. Electron.* **4**, 1−9 (2001).

562   47. Field, A. *Discovering statistics using SPSS* (SAGE, London, 2013)

563   48. Brown, P. Nacurrie 1: Mark of ancient Java, or a caring mother's hands, in terminal

564   Pleistocene Australia?. *Journal of Human Evolution.* **59**, 168-187 (2010)
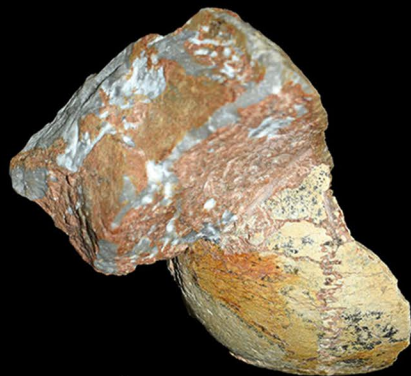
a

Ir2

Sk5

Apidima 1

Qz9

Pt

BH

ES

Sm5

Ir1

Rl

Qz6

Fr1

Om2

Gt

Scc

Ch

Am1

LQ5

Da

PC 2 (14,27% of total variance)

0.015

- 0.02

PC 1
(42,52% of total variance)

posterior   lateral

posterior   lateral

b

Qz9

Adm3

Apidima 1

ES

Om1

Sk5

Scc

Am1

El

Sm5

Ir1

Qz6

Gt

Fr1

Sp1

BH

Rl

Ch

Da

Ir2

Pt

Sp2

Ssc

Bst

Om2

Fh

LQ5

PC 2 (28,11% of total variance)

0.015

- 0.015

PC 1
(43,50% of total variance)

midsagittal profile

midsagittal profile

midsagittal profile

midsagittal profile

c

Qafzeh 6

Petralona   Reilingen   Broken Hill   Irhoud 1   Eliye
Springs

Apidima 1   Skhul 5

Qafzeh 9

Dali   Sima 5   Omo 2   Irhoud 2

-0.08   -0.06   -0.04   -0.02   0   0.02   0.04   0.06   0.08

NEA

MPE   MPA

Apidima 1

AFRICAN
HS

FOSSIL
HS